# Apportioning Light Absorption of Ambient Aerosols to Black Carbon, Brown Carbon, and Lensing Effect Using a PAX-ISS Hybrid Method: Insights into Absorption Enhancement

Yi Shen[1,2], Guorui Zhi[1]*, Wenjing Jin[1], Yao Kong[3], Yuzhe Zhang[1]*, Zhengying Li[4], Jianzhong Sun[5], Yuankai Wang[1], Zhijian Liang[1]

[1]State Key Laboratory of Environmental Criteria and Risk Assessment, Chinese Research Academy of Environmental Sciences, Beijing 100012, China

[2]Department of Atmospheric Science & School of Earth Science, Yunnan University, Kunming 650500, China

[3]Dongying Meteorological Bureau, Dongying 257091, China

[4]Beijing Municipal Ecological and Environmental Monitoring Center, Beijing 100048, China

[5]School of Physical Education, Chizhou University, Chizhou 247000, China.

*Correspondence: Guorui Zhi (zhigr@craes.org.cn) and Yuzhe Zhang (yzzhang943@foxmail.com)

# Abstract

Accurately apportioning aerosol light absorption to black carbon (BC), brown carbon (BrC), and the lensing effect is crucial for constraining aerosol radiative forcing, yet existing methods often fail to resolve all three components simultaneously. Here, we introduce and demonstrate an integrated measurement framework that couples photoacoustic spectroscopy (PAX) with an integrating sphere system using solvent mediation (ISS). This PAX-ISS hybrid method quantifies the total absorption of ambient aerosols ($B_{abs\_coated}$) and removes the lensing effect via solvent-mediated lensing-free optical state to obtain the uncoated absorption ($B_{abs\_uncoated}$). The absorption solely due to the lensing effect ($B_{abs,lensing}$) is then directly quantified as their difference: $B_{abs,lensing}=B_{abs\_coated}-B_{abs\_uncoated}$. $B_{abs\_uncoated}$ is further spectrally decomposed into BC and BrC contributions ($B_{abs,BC}$ and $B_{abs,BrC}$) using a dual-wavelength iterative algorithm. Applied to seasonal samples in Beijing during 2023, the method revealed that BC dominated light absorption, with BrC contributing approximately 10% annually. The apparent lensing-induced enhancement averaged 40% of total absorption but exhibited strong seasonal (4.6–52.0%) and spectral variations, contracting sharply at shorter wavelengths—a pattern ~~indicative~~ suggestive of a BrC "blocking effect" that may offset~~s~~ lensing enhancement. Our field measurements provide~~, for the first time, direct~~ observational ~~evidence supporting~~indications consistent with this blocking effect, which was ~~initially~~ previously proposed by other researchers based ~~solely~~ on numerical simulations. The annual wavelength-averaged absorption enhancement factor ($E_{abs}$) was 1.69 ± 0.10. This methodology provides a robust, observationally constrained approach to apportion aerosol absorption, offering refined insights for climate modeling.

# Graphical Abstract

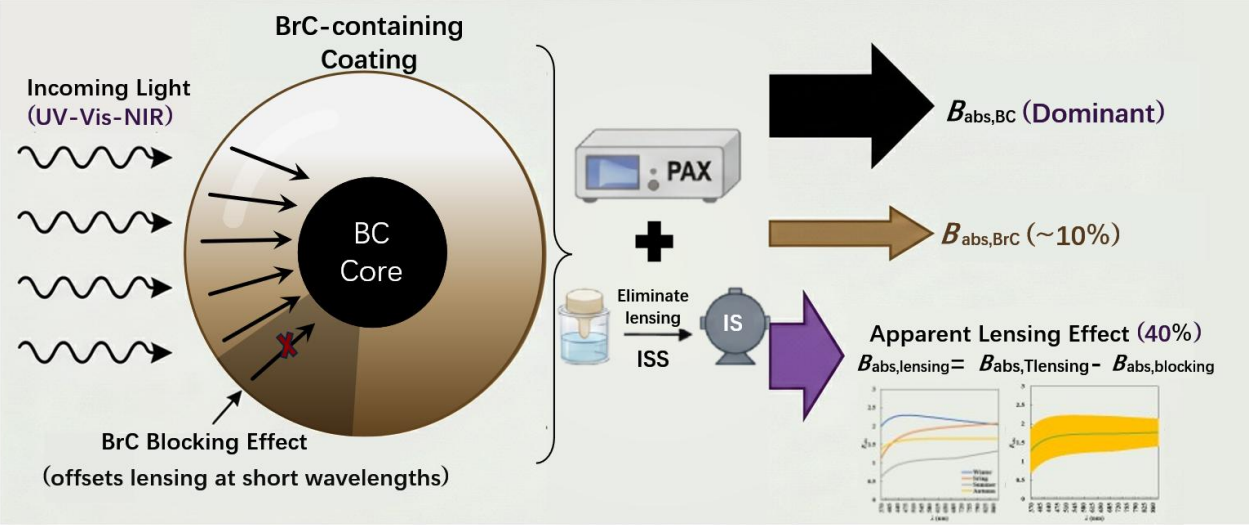

# 1 Introduction

Black carbon (BC) and brown carbon (BrC) are critical components of atmospheric particulate matter due to their strong absorption of solar radiation (Laskin et al., 2025; Xie et al., 2025; Yang et al., 2025). BC is a potent, broad-spectrum absorber, while BrC exhibits strongly wavelength-dependent absorption, primarily in the near-ultraviolet to visible range (Bond et al., 2013; Laskin et al., 2015). Accurately quantifying their respective contributions to total light absorption is fundamental for assessing aerosol radiative forcing, understanding atmospheric heating rates, and constraining climate models (Li et al., 2023a; Yang et al., 2025; Zhu et al., 2021). A key complexity, however, arises from the atmospheric ageing of BC. This process frequently results in the internal mixing of BC with non-absorbing or weakly absorbing coatings and enhances BC's absorption because of the lensing effect (Cappa et al., 2012; Jin et al., 2025; Yus-Díez et al., 2022). Consequently, the total measured absorption coefficient of ambient aerosols ($B_{abs\_coated}$) is an aggregate signal from three distinct physical processes: absorption by bare BC cores, absorption by BrC, and the lensing-driven enhancement of BC absorption due to coatings. Thus, disentangling these three contributors—referred to as apportionment of total aerosol light absorption—is essential for advancing our understanding of aerosol mixing state, ageing processes, and ultimately, climate impacts (Liu et al., 2015; Pokhrel et al., 2017).

However, most methodological frameworks attempting to decompose aerosol total absorption could only resolve one or two of these contributors, but not all three. For example, a common way to obtain the information of one contributor is by accounting for the contributions of the other species based on their own known physicochemical properties. These properties are usually solubility in water or organic reagents or thermal stability at a certain temperature (Cappa et al., 2019; Liu et al., 2015; Xie et al., 2019). For the former, the optical properties of solutions can be measured to estimate the light absorption of BrC (Choudhary et al., 2017; Wu et al., 2019; Yue et al., 2019) and for the latter, BC light absorption can be obtained as organic species are vaporized

(Cappa et al., 2019; Liu et al., 2015; Xie et al., 2019). Being inherently designed to isolate a single component, these approaches typically focus on either BC or BrC alone. Another approach for separating the contributions of BC and BrC from the total measured aerosol light absorption is the absorption Ångström exponent (AAE) attribution method (Lack and Langridge, 2013; Wang et al., 2019a, b). This approach assumes that only BC absorbs solar radiation at near-infrared wavelengths (e.g., 880 nm) and the BC's AAE ($AAE_{BC}$) is 1.0 or other preset values. The light absorptions of BC at other wavelengths ($B_{abs,BC}(\lambda)$) are extrapolated with the help of $AAE_{BC}$, enabling the light absorption of BrC ($B_{abs,BrC}(\lambda)$) to be calculated by subtracting the $B_{abs,BC}(\lambda)$ from the measured total absorption. Considering that the $AAE_{BC}$ value is actually variable (Liu et al., 2018b; Wang et al., 2021b), this approach is not perfect yet.

Thus far, methodological frameworks capable of resolving all three contributors include the applications of pure numerical calculation or the combination of a thermal denuder with a photoacoustic soot spectrometer (PASS-3) in field measurements. The former category is usually embedded with too many assumptions (Luo et al., 2018, 2021; Moschos et al., 2021; Zhang et al., 2021) and needs further improvement based on field verifications. The latter includes the combined use of photoacoustic spectroscopy (PAX) and thermal denuding (TD), which allows for the calculation of an absorption enhancement factor ($E_{abs}$) and, with additional spectral constraints, the separation of BrC and lensing contributions from BC (Cappa et al., 2012; Liu et al., 2015; Pokhrel et al., 2017). Even if the TD process may be subject to an incomplete separation of BrC from BC (Liu et al., 2015) and is therefore not conducive to an accurate apportionment, it is still appreciable in distinguishing the absorption contributors and calculating absorption enhancement factors.

In this study, we introduce and demonstrate an integrated methodological framework designed to apportion total carbonaceous aerosol light absorption into its three constituent parts. Two established but typically separate techniques: PAX and integrating sphere with solvent extraction (ISS) are synergistically coupled to provide

a self-consistent framework to apportion absorption to BC, BrC, and the lensing effect. We present this methodology, detail its implementation, and demonstrate its applications such as in the understanding of absorption enhancement due to absorptive or non-absorptive coatings. We anticipate that this methodology will provide robust constraints for aerosol optical properties and climate modelling.

# 2 **Methodology**

## 2.1 Methodological architecture

As mentioned in the Introduction, the methodology adopted here is based on coupling two mature techniques: PAX and ISS. The PAX provides an accurate, in situ measurement of the total ambient absorption coefficient at 870 nm ($B_{abs\_coated}(870)$) (Lack et al., 2012; Selimovic et al., 2019). This value is subsequently extrapolated to derive $B_{abs\_coated}(\lambda)$ from 380 nm to 880 nm. Concurrently, the ISS system measures the absorption of the same aerosol population after the lensing effect has been eliminated by solvent-mediated coating dissolution and refractive index matching, yielding $B_{abs\_uncoated}(\lambda)$. The reason why the mixed solvent eliminates lensing has been detailed in a few publications (Li et al., 2023b; Sun et al., 2021; Wonaschütz et al., 2009). The difference $[B_{abs\_coated}(\lambda) - B_{abs\_uncoated}(\lambda)]$ directly quantifies the absorption enhancement due solely to the lensing effect ($B_{abs,lensing}(\lambda)$). Furthermore, the ISS system, employing a Double-Wavelength Iterative Calculation (DWIC) algorithm with carbon black and humic acid as reference materials, spectrally decomposes $B_{abs\_uncoated}(\lambda)$ into the contributions of $B_{abs,BC}$ and $B_{abs,BrC}$ (Sun et al., 2021; Wonaschütz et al., 2009). A schematic of the methodological architecture is shown in Figure 1.

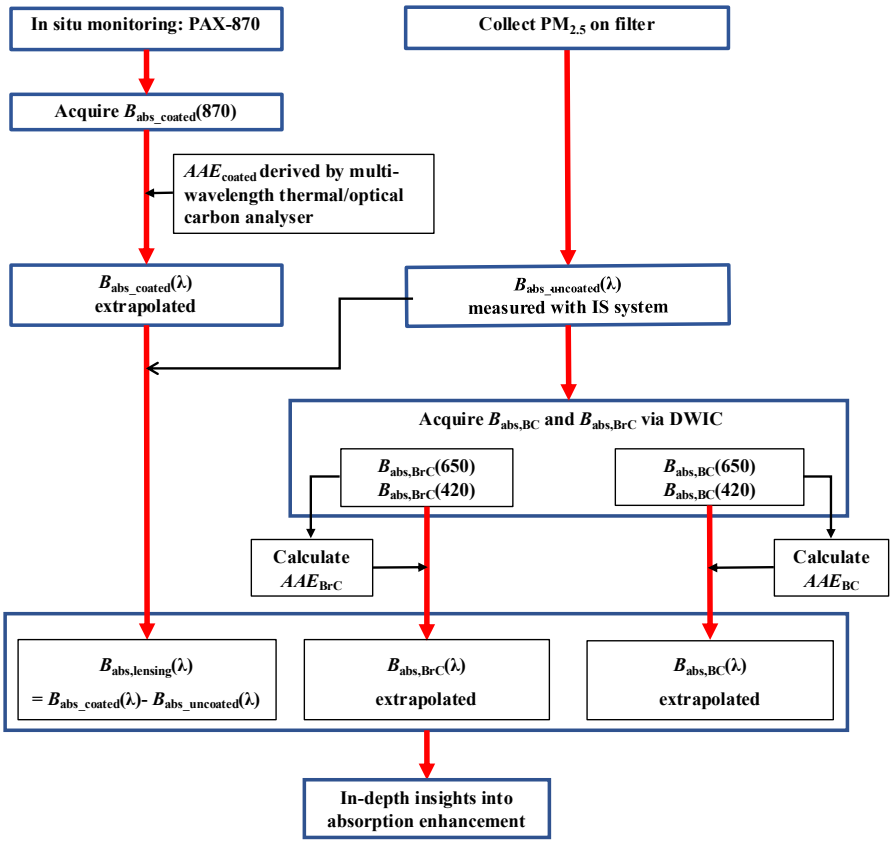


**Figure 1.** Methodological architecture. Note: The λ ranges from 370 nm to 880 nm.

## 2.2 Measurement of lensing-free absorption using ISS system

### 2.2.1 Sample collection

Ambient $PM_{2.5}$ (particulate matter with an aerodynamic diameter ≤ 2.5 μm) was sampled at the Chinese Research Academy of Environmental Sciences (CRAES), Beijing (40.04°N, 116.42°E). A high-volume air sampler (Tisch Environmental Inc., OH, USA) was used at an air flow rate of 1.13 $m^3$/min. The sampling site was situated atop a smog chamber facility (~10 m above ground), with an 80-meter radius free of anthropogenic emission sources nearby (Li et al., 2023b; Wang et al., 2021a; Zhang et al., 2020). Quartz fibre filters (Pallflex™ Tissuquartz 2500QAT-UP, 8″ × 10″, Pall Corporation) were deployed for 23.5-hour repeated sampling cycles, commencing at 09:00 Beijing Time (UTC+8) every day and concluding at 08:30 the following morning. Seasonal campaigns in 2023 spanned the winter period of 9–24 February, the spring period of 7 April–9 May, the summer period of 7 July–6 August, and the autumn period of 12 October–5 November. The selected four time periods are representative of the

meteorological conditions and emission regimes of four quarters of the year (Li et al., 2023b; Wang et al., 2021a; Zhang et al., 2020). The quality assurance measures for sampling filters and eligible days (Table S1) are detailed in the Supplement (Sect. S1).

### 2.2.2 Measurement of absorption for uncoated aerosol

The ISS method was used to measure the absorption for uncoated aerosol. Fischer (1970) first applied the integrating sphere (IS) technique to quantify aerosol absorption. Andre et al. (1981), Heintzenberg (1982), and Hitzenberger et al. (1996) subsequently combined IS with solvent systems, namely ISS, to measure aerosol absorption properties or BC concentrations. Hitzenberger and Tohno (2001) further improved the ISS system by introducing a water/isopropanol rinsing step before acetone dissolution for studies of ambient BC concentrations. After BrC was recognized as an important light-absorbing component, Wonaschütz et al. (2009) used carbon black and humic acid sodium salt as optical reference materials for BC and BrC, respectively, and established the ISS method to distinguish the absorption contributions of BC and BrC in atmospheric aerosols. Sun et al. (2017, 2021) applied the ISS method to samples from residential solid-fuel combustion in China to quantify the emission factors and light-absorption contributions of BC and BrC. More recently, Li et al. (2023b) coupled ISS with in situ PAX absorption observations to quantify differences in absorption efficiency between coated and uncoated aerosols and explicitly described the mechanism as “de-lensing through solvent dissolution and solvent de-refraction”.

As previously described, the ISS system eliminates $B_{\mathrm{abs,lensing}}(\lambda)$ while preserving bare BC and BrC absorption components (i.e., $B_{\mathrm{abs\_uncoated}}(\lambda) = B_{\mathrm{abs,BC}}(\lambda) + B_{\mathrm{abs,BrC}}(\lambda)$) (Sun et al., 2017; Wonaschütz et al., 2009; Li et al., 2023b). The system comprises a light source, a custom-made 150 mm IS, and a UV–Vis-NIR spectrometer (Li et al., 2023b; Sun et al., 2017, 2021; Wang et al., 2021a). For each measurement, a transparent quartz cuvette (1 cm × 1 cm × 4 cm), holding 3 mL of a solvent mixture (acetone, water, and 2-propanol in a ratio of 5:4:1) was fixed in the center of the integrating sphere chamber. A filter punch (30×8 mm) was immersed in the solvent

mixture within the cuvette for optical detection. The wavelength-resolved absorbance ($ABS_{ISS}(\lambda)$) was acquired from 370 nm to 880 nm, defined as:

$$ABS_{ISS}(\lambda) = -ln\frac{I(\lambda)}{I_0(\lambda)}, \quad (1)$$

where $I(\lambda)$ and $I_0(\lambda)$ denote the transmitted light intensities through the loaded and blank filters, respectively. $B_{abs\_uncoated}(\lambda)$ is then converted as:

$$B_{abs\_uncoated}(\lambda) = \frac{100 \times ABS_{ISS} \times A}{CF \times F \times T}, \quad (2)$$

where $A$ is the total deposited area on the filter used by the high-volume sampler described in Sect. 2.2.1 ($cm^2$); $F$ is the flow rate of filter sampling ($m^3$/min); $T$ is the duration of each filter sampling (min); and $CF$ is the correction factor converting the ISS-measured absorption (multiple-angle absorption within the integrating sphere chamber) to the conventional one-way absorption (as measured by PAX). The method for determining the $CF$ value has been described in our previous publication (Li et al., 2023b) and is represented in the Supplement (Sect. S2).

## 2.3 Measurement of total absorption via PAX

### 2.3.1 Thermal/optical analysis

A DRI Model 2015 Multi-Wavelength Thermal-Optical Carbon Analyser was used to split aerosol total carbon (TC) into organic carbon (OC) and elemental carbon (EC) employing temperature-regulated pyrolysis under controlled atmospheres. A 0.5024 $cm^2$ punch from a quartz filter was heated stepwise to 140 °C (OC1), 280 °C (OC2), 480 °C (OC3), and 580 °C (OC4) in a pure helium atmosphere and then combusted stepwise at 580 °C (EC1), 740 °C (EC2), and 840 °C (EC3) in a 2% oxygen + 98% helium atmosphere following the IMPROVE_A temperature protocol. The mass values of OC and EC were calculated as OC = OC1 + OC2 + OC3 + OC4 + OPC and EC = EC1 + EC2 + EC3 - OPC, where OPC represents pyrolyzed OC (Chow et al., 2007).

To acquire *AAE*s, filter transmittance and reflectance were continuously monitored using 7-wavelength diode lasers (405, 445, 532, 635, 780, 808, 980 nm), and the wavelength-specific light attenuation (*ATN*) was calculated accordingly. To mitigate filter matrix artefacts, including loading effects and multiple scattering (Chen et al.,

2015; Chow et al., 2018; Peng et al., 2020), wavelength- and EC loading-dependent adjustment factors were applied to the raw *ATN* to obtain corrected *ATN*s (see Supporting Information Sect. S3, Table S2). Based on these, the *AAE*s for coated aerosols ($AAE_{coated}$) were calculated. The $AAE_{coated}$ was then used to extrapolate $B_{abs\_coated}(\lambda)$ from $B_{abs\_coated}(870)$ in the following section.

### 2.3.2 Acquisition of total absorption at broad wavelength range

A photoacoustic extinction spectrometer (PAX-870, Droplet Measurement Technologies) was deployed to monitor the in situ atmospheric $B_{abs\_coated}(870)$ in real-time. Considering that we have only a PAX set with a single wavelength (870 nm), $B_{abs\_coated}(\lambda)$ had to be extrapolated using the $AAE_{coated}$ obtained in Sect. 2.3.1:

$$B_{abs\_coated}(\lambda) = B_{abs\_coated}(870) \times \left(\frac{\lambda}{870}\right)^{-AAE_{coated}} \quad (3)$$

It should be noted that extrapolating the single-wavelength measurement of PAX to other wavelengths is a source of uncertainty, which is specifically considered in Section 3.4. To minimize the potential bias caused by differences in filter substrates, the same batch of quartz filters were used for both thermal/optical analysis and integrating sphere measurements in this study.

## 2.4 Decomposition of coated aerosol absorption by coupling ISS-PAX

### 2.4.1 Lensing-equivalent absorption

The availability of $B_{abs\_coated}(\lambda)$ from PAX and $B_{abs\_uncoated}(\lambda)$ from ISS allows the acquisition of $B_{abs,lensing}(\lambda)$. As shown in Figure 1, $B_{abs,lensing}(\lambda)$ is obtained by calculating the difference between $B_{abs\_coated}(\lambda)$ and $B_{abs\_uncoated}(\lambda)$, as:

$$B_{abs,lensing}(\lambda) = B_{abs\_coated}(\lambda) - B_{abs\_uncoated}(\lambda) \quad (4)$$

Within this framework, the online PAX observations and offline filter-based ISS measurements share a common basis of daily-integrated aerosol populations (23.5 h/day, allowing 30 minutes for filter replacement) from the same sampling site and size range, rather than a strict match of instantaneous aerosol populations. The quality control procedures for the ISS-PAX system processing are detailed in Section S5 of the Supplement.

Although the two data streams are matched on the same daily sampling window, intraday variability is not resolved by this framework. $AAE_{coated}$ is derived from a daily-integrated filter, whereas PAX measures $B_{abs\_coated}(870)$ at high temporal resolution before being averaged over the corresponding 23.5 h period. If $AAE_{coated}$ and $B_{abs\_coated}(870)$ covary substantially within a day, applying a single daily $AAE_{coated}$ to the daily-averaged PAX value may smooth this covariance and introduce bias into the reconstructed daily spectrum. Accordingly, the present results are interpreted at daily and longer (seasonal and annual) time scales rather than in terms of diurnal variability.

### 2.4.2 BC and BrC absorptions

To decompose $B_{abs\_uncoated}(\lambda)$, which is lensing free, into the individual contributions of BC and BrC, the DWIC algorithm was employed. Details of the DWIC algorithm have been described in our previous publications (Sun et al., 2017, 2021; Wang et al., 2021a) and in the Supplement (Sect. S4 and Figure S1). Briefly, the iterative calculation uses two wavelengths (650 and 420 nm) and two reference materials: Carbon Black (CarB) as the proxy for BC, and Humic Acid Sodium Salt (HASS) as the proxy for BrC (Reisinger et al., 2008; Sun et al., 2017; Wang et al., 2021a; Wonaschütz et al., 2009). CarB was used as proxy for BC in diesel exhaust by Medalia et al. (1983) and HASS was used as proxy for BrC in wood combustion by Wonaschütz et al. (2009). In two previous studies conducted by our team, CarB and HASS were used as proxies for BC and BrC, respectively, from residential solid-fuel combustion (Sun et al., 2017; 2021). We carried over this philosophy to the current study. Calibration curves for CarB and HASS masses were established based on their respective absorption signals measured by the ISS at 650 (BC-dominated) and 420 nm (BrC-sensitive). Iterative optimization yielded the absorption coefficients of BC and BrC at these two wavelengths, i.e., $B_{abs,BC}(650)$, $B_{abs,BC}(420)$, $B_{abs,BrC}(650)$, and $B_{abs,BrC}(420)$.

The absorption coefficients of BC and BrC at wavelengths other than 420 nm and 650 nm (i.e., $B_{abs,BC}(\lambda)$, $B_{abs,BrC}(\lambda)$) can be extrapolated from the values at these two wavelengths, constrained by their respective *AAE*s ($AAE_{BC}$ and $AAE_{BrC}$). The *AAE* for

BC or BrC is calculated as:

$$AAE_{\mathrm{X}} = -\frac{\ln\left(\frac{B_{\mathrm{abs,x}}(650)}{B_{\mathrm{abs,x}}(420)}\right)}{\ln\frac{650}{420}} \quad (5)$$

The absorption coefficient at any wavelength is then given by:

$$B_{\mathrm{abs,x}}(\lambda) = B_{\mathrm{abs\_uncoated}}(420) \times \left(\frac{\lambda}{420}\right)^{-AAE_{\mathrm{X}}} \quad (6)$$

where X refers to BC or BrC. The wavelength 420 nm in Eq. (6) can be replaced by 650 nm. Note that the selection of 420 and 650 nm was based mainly on the following considerations. The wavelength 420 nm lies in the short-wavelength region of visible light, where BrC has much higher light-absorption efficiency than at 650 nm; thus, it can serve as a BrC-sensitive wavelength. By contrast, 650 nm lies in the longer-wavelength visible region, where BrC absorption is much weaker than at 420 nm, whereas BC still maintains strong absorption. Therefore, 650 nm can be regarded as a BC-dominated wavelength. However, this does not exclude other wavelength pairs than the 650-420 pair only if they have sufficient spectral separation, different sensitivities to BC and BrC absorption, and stable light-intensity signals.

### 2.5 Calculation of absorption enhancement factors

With the total aerosol absorption apportioned to BC, BrC, and lensing effect, the absorption enhancement factor of BC ($E_{\mathrm{abs}}(\lambda)$) is available via:

$$E_{\mathrm{abs}}(\lambda) = \frac{B_{\mathrm{abs,BC}}(\lambda) + B_{\mathrm{abs,lensing}}(\lambda)}{B_{\mathrm{abs,BC}}(\lambda)} \quad (7)$$

## 3 Results and discussion

### 3.1 Concentrations and total absorptions of ambient aerosol

#### 3.1.1 Concentrations

Every filter-collected sample was weighed to determine $PM_{2.5}$ concentration and analysed for aerosol carbon speciation (Figure 2). Representative seasonal heterogeneity was observed in aerosol loadings and compositions.

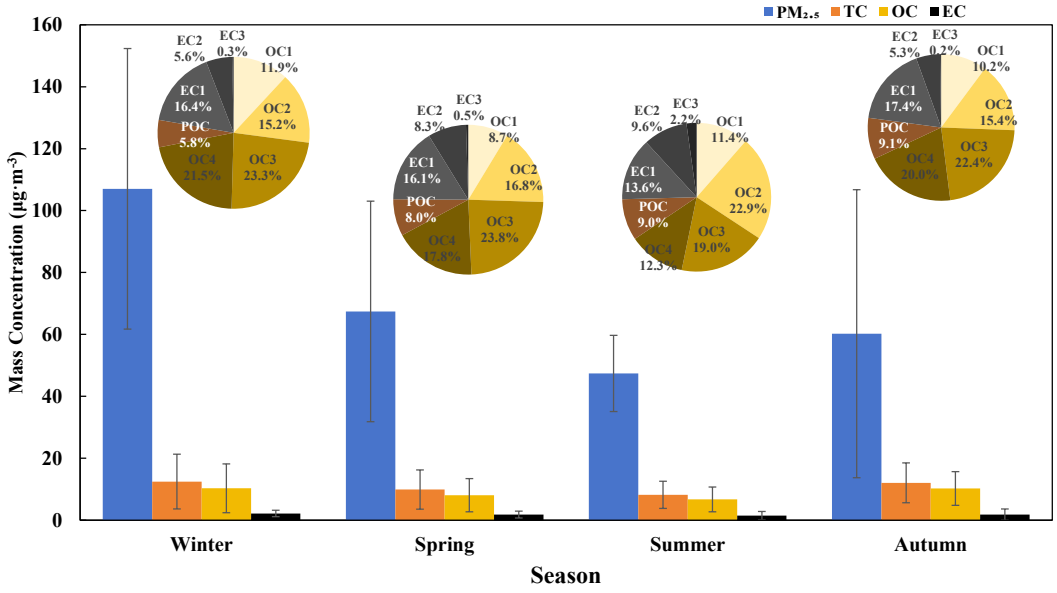


**Figure 2.** Aerosol loadings and compositions in 2023.

As shown in Figure 2, $PM_{2.5}$ mass concentrations demonstrate pronounced seasonal variations, peaking in winter ($107.03 \pm 45.31$ μg·m$^{-3}$) and reaching a minimum in summer ($47.40 \pm 12.30$ μg·m$^{-3}$), consistent with regional emission patterns and meteorological conditions (Chen et al., 2017; Wu et al., 2016b). The seasonal trends in TC, OC, and EC concentrations generally mirrored those of $PM_{2.5}$, although the relative order of spring and autumn was occasionally reversed. For example, unlike $PM_{2.5}$ concentrations of spring > autumn, EC concentrations are of autumn > spring, implying differences in $PM_{2.5}$ composition arising from varied sources, transport, and ageing processes (Arhami et al., 2018; Ravindra et al., 2022; Song et al., 2022).

Thermal-optical carbon analysis provided distinct source signatures, as indicated by the char-EC/soot-EC ratios. Elevated ratios during high-combustion seasons like winter ($1.81 \pm 1.61$) and autumn ($1.50 \pm 2.67$) reflect predominant contributions from coal and biomass burning, as established by source apportionment studies (e.g., Han et al., 2010). In contrast, reduced ratios during spring ($0.93 \pm 0.77$) and summer ($0.39 \pm 0.58$) accord with vehicular-dominated emissions (Han et al., 2008; Liu et al., 2018a). Further speciation of OC to OC1, OC2, OC3, and OC4 suggests the influence of atmospheric processing. Low-volatility OC3–OC4 fractions constitute 40–54% of total OC across all seasons, indicating the pathways of photochemical ageing and aqueous-

phase processing that generate oxygenated semi-volatile compounds (Aswini et al., 2019; Li et al., 2018).

### 3.1.2 Total absorption

Having established the mass concentration and compositional context, we now examine the optical absorption properties of the coated aerosols. The daily light absorption of coated aerosol calculated in Sect. 2.3.2 was averaged seasonally and annually. Figure 3 shows the spectral dependence of $B_{abs\_coated}(\lambda)$ across seasons and the annual average. Both the absorption intensity and $AAE_{coated}$ exhibit a consistent seasonal order: winter > autumn > spring > summer. This order aligns with the seasonal trend in TC concentrations shown in Figure 2. Since both BC and BrC are spectrally dependent components of TC, it is consistent that the $AAE_{coated}$ values follow the same order as TC concentrations.

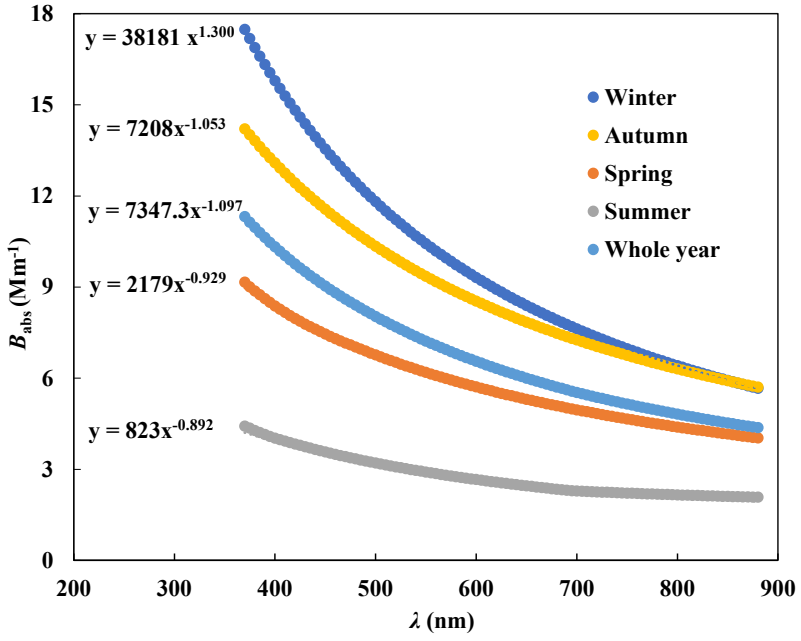


**Figure 3.** Total absorption of coated aerosol.

The $AAE_{coated}$ values were highest in winter (1.300) and lowest in summer (0.892), with an annual mean of 1.053. *AAE*s lower than 1.0 are observed in spring and summer, seemingly challenging the traditional view that the *AAE* of carbonaceous aerosol should exceed 1.0, given that BC's *AAE* is typically 1.0 and BrC's *AAE* >1.0 (Lack and Langridge, 2013). However, previous source-related experiments and Mie model

calculations (Li et al., 2016; Liu et al., 2018b; Wang et al., 2021b) have reported a wide range of values for $AAE_{BC}$ (e.g., 0.6−1.6) due to various confounding factors (e.g., aerosol size distributions, morphology, mixing state, or core-shell structure, etc.) (Curci et al., 2019; Guan et al., 2026; Helin et al., 2021; Liu et al., 2018b; Zhang et al., 2020), implying the possibility of *AAE* values below 1.0 for coated aerosol. While referencing this broad range is instructive, the consistently low $AAE_{coated}$ values in our spring and summer data may also be partially influenced by the net spectral effect of lensing enhancement and BrC blocking, which our subsequent deconvolution analyses aim to clarify.

To sum up this section (Sect. 3.1), the distinct seasonal characteristics of aerosol concentrations, carbon ratios, and *AAE*s reflect the diversity of the local ambient aerosol population, providing a suitable context for a comprehensive study of overall and decomposed light absorptions using the PAX-ISS hybrid method.

## 3.2 Deconvolved light absorption

$B_{abs\_coated}(\lambda)$ was deconvolved into $B_{abs,BC}(\lambda)$, $B_{abs,BrC}(\lambda)$, and $B_{abs,lensing}(\lambda)$ on daily, seasonal, and annual bases. Figure 4 shows the seasonal and annual decomposed absorption, where panels a−d display the wavelength-resolved contributions for winter, spring, summer, and autumn, respectively; panel e shows the annual wavelength-resolved contribution; and panel f shows the wavelength-averaged contributions for each season and the whole year. As noted, the wavelength range considered spans 370−880 nm, representing a most energetic part of solar radiation (Thuillier et al., 2003). To enable direct comparison across time periods, all panels showing wavelength-resolved absorptions (a−e) share a common y-axis upper limit of 18 $Mm^{-1}$.

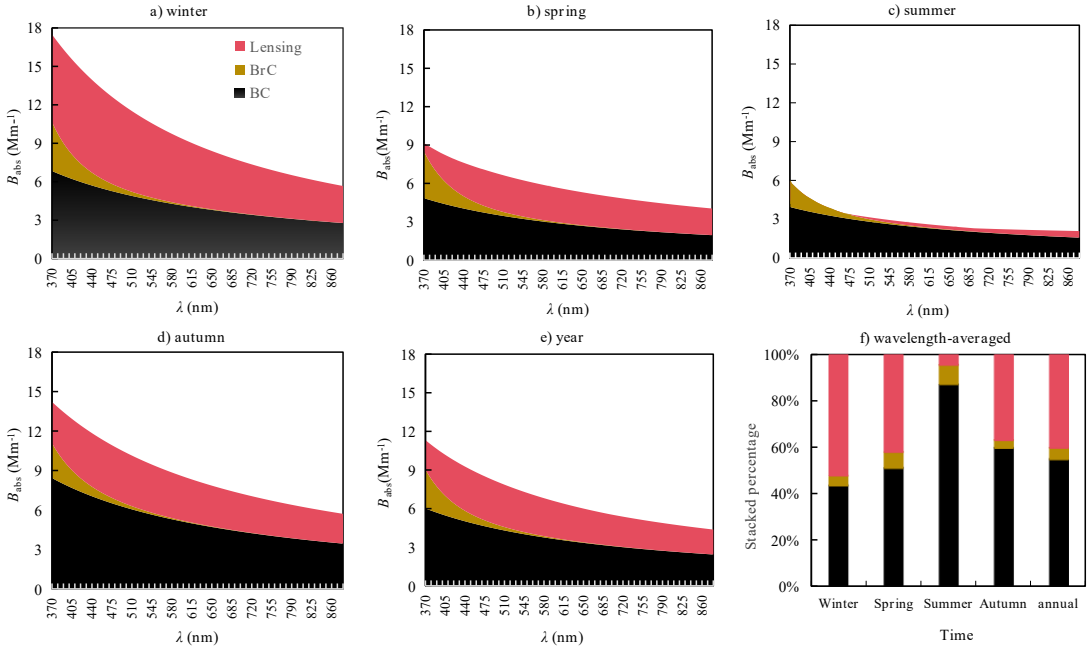


**Figure 4.** Deconvolved aerosol light absorption in wavelength-resolved (a—e) and wavelength-averaged (f) forms.

Both BC and BrC exhibited clear spectral dependence seasonally and annually (panels a—e), with BrC's dependence being more pronounced than BC's, consistent with the established knowledge that $AAE_{BrC} > AAE_{BC}$ (Kaskaoutis et al., 2021; Lack and Langridge, 2013; Wu et al., 2016a). In all seasons, BC absorption exceeded BrC absorption even at ultraviolet wavelengths, indicating BC's dominant role in light absorption for the urban aerosol studied. This is further corroborated by Figure 4f, where the wavelength-averaged BrC absorption value was approximately 10% of BC absorption value for both individual seasons and the annual average. Regarding $B_{abs,lensing}$, Figure 4f shows an annual mean contribution of 40.0% to $B_{abs\_coated}$, with seasonal means of 52.0% in winter, 41.8% in spring, 4.6% in summer, and 36.7% in autumn. These differing seasonal contributions of $B_{abs,lensing}$ suggest varying degrees of BC absorption enhancement, discussed in Sect. 3.3.

More significantly, and central to one of our key findings, Figure 4a—e reveals a pronounced contraction of the apparent lensing effect toward shorter wavelengths. For example, at the annual level (Figure 4e), the lensing-equivalent absorption at 370 nm was only 66.3% of its maximum value at 455 nm. In spring (Figure 4b), lensing-equivalent absorption at 370 nm shrank to 22.9% of the maximum at 505 nm. The most

extreme case was observed in summer (Figure 4c), where the lensing-equivalent absorption disappears at wavelengths below 465 nm. In this scenario, the summed absorption of BC and BrC at specific wavelengths (e.g., below 465 nm) exceeded the total measured absorption (summed absorption of BC, BrC, and lensing), suggesting that the intrinsic total lensing effect ($B_{\mathrm{abs,Tlensing}}$) was overbalanced by other factors to the extent that $B_{\mathrm{abs,lensing}}$ became negligible or negative. Although an accurate and reliable explanation for this spectral contraction phenomenon remains unavailable, the multiple effects of BrC internally mixed with BC cores are attracting increasing attention. Generally, coatings on BC can enhance its absorption via the lensing effect. When coatings are themselves absorptive (e.g., BrC), this enhancement constitutes one of the largest uncertainties in estimating aerosol radiative forcing (e.g., Curci et al., 2019; Wang et al., 2018). It has been established that the absorption enhancement of BC due to absorptive coatings (BrC) is lower than that induced by non-absorbing coatings (Lack and Cappa, 2010).

Further studies propose classifying BrC's impacts on BC absorption into a BrC-induced lensing effect and a BrC blocking effect (Luo et al., 2018; Zhang et al., 2021). In our framework, the lensing effect caused by BrC combines with that from non-absorbing coatings to constitute the intrinsic $B_{\mathrm{abs,Tlensing}}$. The blocking effect ($B_{\mathrm{abs,blocking}}$) occurs when BrC coatings block some photons that would otherwise be focused onto the BC core by the lensing effect, akin to a shadow. Therefore, total aerosol absorption should be defined as:

$$B_{\mathrm{abs\_coated}} = B_{\mathrm{abs,BC}}(\lambda) + B_{\mathrm{abs,BrC}}(\lambda) + \left(B_{\mathrm{abs,Tlensing}}(\lambda) - B_{\mathrm{abs,blocking}}(\lambda)\right) \quad (8)$$

Consequently, $B_{\mathrm{abs,lensing}}$ we measured represents the net balance between $B_{\mathrm{abs,Tlensing}}(\lambda)$ and $B_{\mathrm{abs,blocking}}$. Accordingly, $B_{\mathrm{abs,lensing}}(\lambda)$ becomes negative whenever $B_{\mathrm{abs,blocking}}(\lambda)$ exceeds $B_{\mathrm{abs,Tlensing}}(\lambda)$. Thus, the observed contraction of $B_{\mathrm{abs,lensing}}$ in Figure 4, which is precisely ($B_{\mathrm{abs,Tlensing}}$ – $B_{\mathrm{abs,blocking}}$), is not surprising. The disappearance of $B_{\mathrm{abs,lensing}}(\lambda)$ in summer below 465 nm (Figure 4c) likely does not indicate the absence of intrinsic total lensing but rather suggests that $B_{\mathrm{abs,Tlensing}}(\lambda)$ –

$B_{abs,blocking}(\lambda) \leq 0$. The plausibility of such a BrC-induced blocking effect is supported by prior numerical investigations. For instance, Luo et al. (2018), employing the multiple-sphere T-matrix (MSTM) method, demonstrated that the total absorption of a BC core with brown coatings can be less than the sum of separately calculated absorptions ($B_{abs,BC} + B_{abs,BrC}$), attributable to blocking. Similarly, Zhang et al. (2021) numerically found that the lensing effect may not increase further with shell/core ratio beyond a threshold due to blocking. Furthermore, the wavelength dependence of the apparent lensing in Figure 4 (apparent lensing decreases toward shorter wavelengths) is largely complementary to that of BrC absorption (BrC absorption increases toward shorter wavelengths), implying an interplay with BrC blocking effects. Further investigations are needed to clarify the conditions for blocking effects, their interaction with the lensing from non-absorptive coatings, and their relationship with the direct light absorption from BrC.

## 3.3 Insight into absorption enhancement

The absorption enhancement of BC due to lensing is considered one of the largest uncertainties in assessing the climate impact of aerosol light absorption (Fan et al., 2024; Kong et al., 2024; Zhao et al., 2021). Here, we examine absorption enhancement from both wavelength-resolved and wavelength-averaged perspectives, followed by a discussion of why some enhancement quantification methods require correction.

### 3.3.1 Wavelength-resolved enhancement: insight into blocking effects

Using the daily wavelength-resolved absorption coefficients of BC, BrC, and apparent lensing effect (i.e., $B_{abs,BC}(\lambda)$, $B_{abs,BrC}(\lambda)$, and $B_{abs,lensing}(\lambda)$) obtained via Eqs. (4) and (6), the daily, seasonal, and annual wavelength-resolved enhancement factors ($E_{abs}(\lambda)$) were calculated using Eq. (7).

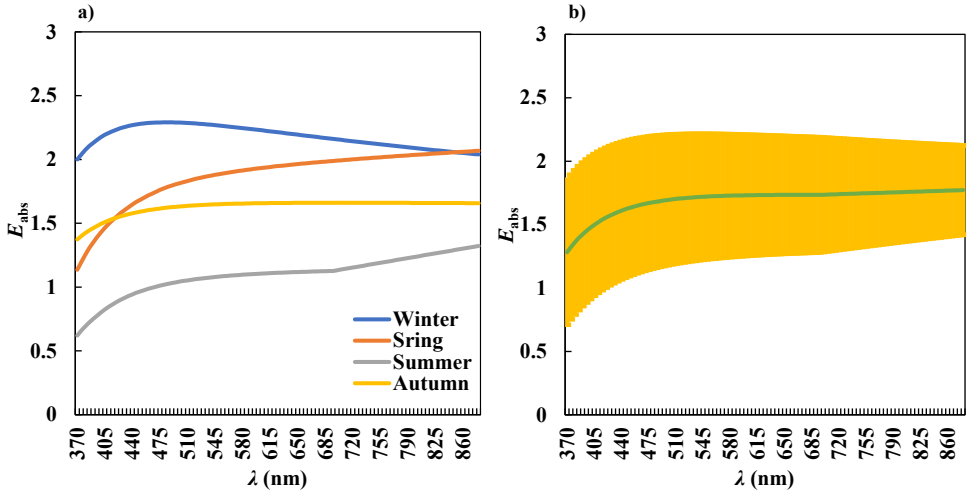


**Figure 5.** Averaged absorption enhancement factors for seasonal (a) and yearly (b) terms.

Figure 5 shows the wavelength-resolved enhancement factors for the seasons and the year. A clear wavelength dependence is evident. Specifically, $E_{abs}(\lambda)$ decreased monotonically toward shorter wavelengths in spring, summer, and autumn, while in winter it increased initially before declining in the short-wavelength range. That is, all seasonal and annual $E_{abs}(\lambda)$ values turned downward as wavelengths approached the violet range. The observed decline in $E_{abs}(\lambda)$ is mechanistically explained by the definition of $E_{abs}$ ($E_{abs} = 1 + B_{abs,lensing}/B_{abs,BC}$) given the concurrent decrease in $B_{abs,lensing}$ (Figure 5) and the increase in $B_{abs,BC}$ at shorter wavelengths (Figure 4). This decline in $E_{abs}$ at short wavelengths is ~~thus fundamentally driven by~~likely associated with the strengthened blocking effect of BrC coatings, which reduces the net apparent lensing ($B_{abs,lensing} = B_{abs,Tlensing} - B_{abs,blocking}$). The most extreme case occurred in summer at wavelengths below 465 nm, where observed $E_{abs}(\lambda)$ values fell below 1.0, indicating that the net apparent lensing contributed negatively to BC light absorption. This ~~echoes~~ is consistent with the finding of Luo et al. (2018) that $E_{abs}(\lambda)$ can be below 1 in the ultraviolet region for BC with brown coatings due to blocking, which they termed the "sunglasses effect". While the blocking effect of BrC has previously been examined ~~only~~ mainly through numerical simulations (e.g., Luo et al., 2018; Zhang et al., 2021), ~~our study provides the first field-based evidence to demonstrate this phenomenon.~~our results provide suggestive field-based evidence consistent with this phenomenon rather

than definitive proof of the underlying mechanism

### 3.3.2 Wavelength-averaged enhancement: insight into pollution-enhancement linkage

Theoretical and experimental studies of lensing-induced absorption enhancement have yielded diverse results. Mie theory for spherical core-shell particles yields enhancement factors up to 3 (Bond et al., 2006; Jacobson, 2001; Schwarz et al., 2008). Such enhancement is supported by laboratory studies (Cappa et al., 2012; Schnaiter, 2005; Shiraiwa et al., 2010; Zhang et al., 2008) and is incorporated into climate models that work out total BC absorption (lensing included) either through simplified mixing-state assumptions (Chung, 2005; Penner et al., 1998) or by fixing the enhancement value at ~1.5 (Flanner et al., 2007; Wang et al., 2014). In contrast, some field measurements have reported negligible absorption enhancement for ambient BC particles (Cappa et al., 2012, 2019; Fierce et al., 2016; Mbengue et al., 2021).

Complementing the wavelength-resolved results, we present the wavelength-averaged enhancement factor ($E_{abs}$, averaged over 370-880 nm) to assess the overall status of lensing. As shown in Figure 6, the annual average $E_{abs}$ was 1.69 ± 0.10. Seasonal averages varied from 1.09 ± 0.15 (summer) to 2.18 ± 0.08 (winter), with spring and autumn values of 1.81 ± 0.21 and 1.63 ± 0.06, respectively. Given the decisive role of lensing, the considerable seasonal divergence in $E_{abs}$ is attributable to the varying contributions of $B_{abs,lensing}$ to $B_{abs\_coated}$ (e.g., 4.6% in summer versus 52.0% in winter; see Figure 4f). Other researchers have also reported diverse absorption enhancement factors in China, depending on specific conditions influencing lensing, particularly aerosol ageing statuses (Luo et al., 2018). For example, Cui et al. (2016) reported factors of 1.4 ± 0.3 for fresh combustion and ~3 for aged BC at a rural North China Plain site. Chen et al. (2017) reported an average of 2.07 ± 0.72 for winter haze in northern China, with diurnal variation from 1.31±0.29 (morning) to 2.23±1.05 (afternoon) and 1.52±0.75 (evening). Xu et al. (2016) even reported $E_{abs}$ values of 2.6–4.0 for Beijing. Note that the definitions of $E_{abs}$ vary a little in literature depending upon

how to remove coatings or how to deal with BrC (a comprehensive comparison on different operational definitions is provided in Section S6 of the Supplement).

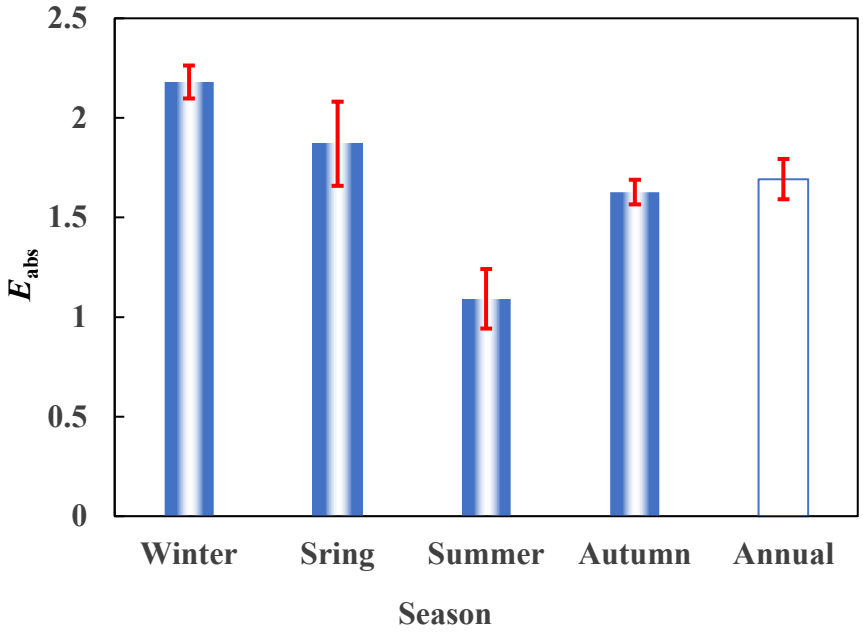


**Figure 6.** Wavelength-averaged absorption enhancement factors for seasons and the year.

Beyond the comparison with literature values, a notable pattern emerges within our dataset: the seasonal $E_{abs}$ values (Figure 6) vary synchronously with $PM_{2.5}$ concentrations (Figure 2); that is, higher $PM_{2.5}$ levels corresponded to higher absorption enhancement factors. This aligns with our previous findings that increased air pollution leads to greater absorption enhancement (Li et al., 2023b; Zhang et al., 2017, 2020; Zhi et al., 2014). Increased air pollution in northern China usually results from stagnant weather that favors aerosol ageing, leading to the accumulation of primary emissions and the formation of secondary aerosols (Liu et al., 2024; Peng et al., 2021). The increased load of inorganic and organic pollutants enhances the likelihood and thickness of coatings on BC, thereby boosting the lensing effect (Li et al., 2023b).

This positive correlation is supported by the enhanced abundance of low-volatility, oxidised organic components (OC3-OC4, see Figure 2) during the high-$PM_{2.5}$ seasons (winter and autumn). These components are markers of atmospheric ageing and secondary formation (Boonpeng et al., 2026; Chow et al., 2007; Tohidi et al., 2022), processes conducive to the development of thicker coatings on BC, thereby promoting

457 a stronger lensing effect.

458 With sustained improvements in local air quality in China, conflicting climate
459 influences may emerge: the warming effect could weaken due to a continued decline of
460 $E_{abs}$, while the cooling effect from aerosol scattering could also weaken due to declining
461 $PM_{2.5}$ concentration (Kelesidis et al., 2022; Samset et al., 2025; Xie et al., 2025). Future
462 work should address this potential contradiction.

463 ## 3.4 Assessment of uncertainties

464 The derivation of $E_{abs}(\lambda)$ using the PAX-ISS method involves multiple technical
465 procedures and steps; consequently, its overall uncertainty is derived through the
466 propagation of uncertainties from the associated sub-variables. A detailed description
467 of the principles, methodologies, and results regarding the uncertainty estimation for
468 $E_{abs}(\lambda)$ is provided in the Supplement. After the uncertainties of $B_{abs\_coated}(870)$,
469 $AAE_{coated}$ $ABS_{ISS}$, CF, and $B_{abs,BC}(\lambda)$ were identified, the Monte Carlo simulation is
470 used to calculate the probability distribution of the $E_{abs}$ for a sample on February, 19,
471 2023. As a result, at 420 nm, the mean $E_{abs}$ is $1.789 \pm 0.221$, corresponding to an
472 uncertainty of 12.4%. At 650 nm, the mean $E_{abs}$ is $2.324 \pm 0.189$, corresponding to an
473 uncertainty of 8.1% (Figure 7). The Monte Carlo simulation is also used to calculate
474 the probability distribution of the $B_{abs,lensing}(\lambda)$ for the sample on February, 19, 2023,
475 which is detailed in Section S7 of the Supplement.

476 The propagated uncertainties above do not necessarily encompass all systematic
477 effects associated with the filter-derived $AAE_{coated}$. Residual positive or negative filter
478 artefacts and possible sampling-induced changes in particle morphology, if present,
479 could propagate through the extrapolated $B_{abs\_coated}(\lambda)$ into $B_{abs,lensing}(\lambda)$ and $E_{abs}(\lambda)$.
480 Such effects are expected to be more consequential at wavelengths farther from the
481 directly measured 870 nm PAX channel. Therefore, the exact magnitude and spectral
482 dependence of the short-wavelength enhancement are interpreted cautiously.

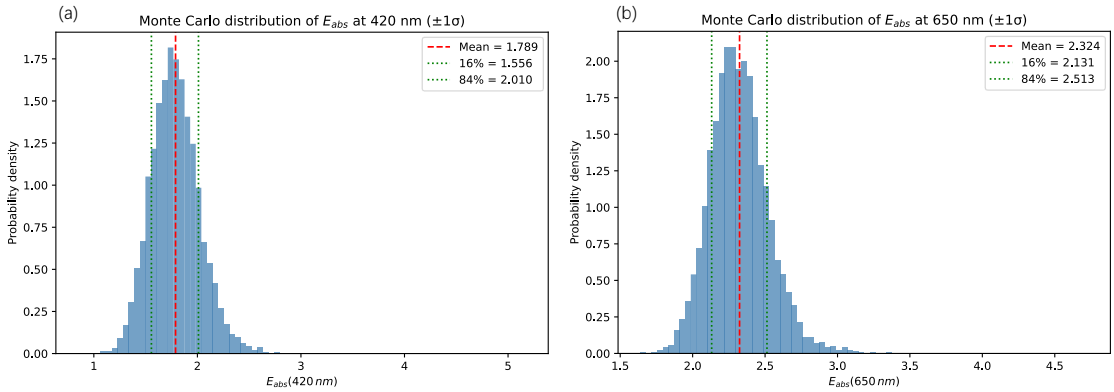


**Figure 7**. Probability distribution of $E_{abs}$ at 420nm (a) and 650nm (b) on 19 February 2023. The ±1σ range (68% probability) is used to represent uncertainty.

# 4 Conclusions

This study developed and applied a novel hybrid measurement method, coupling in situ PAX with filter-based ISS, to quantitatively apportion ambient aerosol light absorption into contributions from BC, BrC, and the lensing effect. The method successfully provided a self-consistent, observationally constrained pathway to separate these three components, addressing a persistent challenge in atmospheric aerosol science.

Key findings from the annual and seasonal analysis of Beijing aerosols in 2023 include:

**(1) Successful Apportionment:** The PAX-ISS method successfully deconvolved the total absorption, confirming BC as the dominant absorber. BrC contributed approximately 10% to the annual wavelength-averaged absorption, highlighting its non-negligible role even in an urban environment.

**(2) Spectral Nature and Seasonal Variability of Lensing:** The lensing-induced enhancement accounted for an annual average of 40.0% of total absorption but showed profound seasonal variability (winter: 52.0%; summer: 4.6%). Crucially, $B_{abs,lensing}$ exhibited strong spectral dependence, contracting significantly at shorter wavelengths (UV/blue). This contraction is inconsistent with a purely additive lensing model.

**(3) Observational ~~Evidence~~ Indication ~~for~~ of the BrC Blocking Effect:** The observed spectral contraction, particularly the near-zero or negative apparent lensing at

short wavelengths in summer, suggests a ~~provides compelling~~ field-based ~~evidence for a~~indication of a "blocking effect" ~~caused by~~associated with absorptive BrC coatings on BC cores. This effect may partially offset~~s~~ the traditional lensing enhancement and influence~~, leading to~~ the net apparent lensing captured by our method ($B_{abs,lensing}$ = $B_{abs,Tlensing} - B_{abs,blocking}$). Our results are consistent with~~align with and provide tangible support for~~ previous theoretical and numerical studies proposing this mechanism, while further investigations are needed to directly verify the controlling processes.

**(4) Absorption Enhancement Factors and Pollution Linkage:** The derived wavelength-averaged $E_{abs}$ varied seasonally from 1.09 ± 0.15 (summer) to 2.18 ± 0.08 (winter), with an annual mean of 1.69 ± 0.10. These values correlated with seasonal $PM_{2.5}$ levels, linking stronger enhancement to more polluted, aged aerosol conditions.

**(5) Caveats and Limitations:** The PAX-ISS hybrid method offers a powerful tool for deconvolving the complex sources of aerosol absorption without requiring detailed assumptions or information about particle microphysical properties, such as size distributions, morphology, mixing state, or core-shell structure. This characteristic is, on one hand, an advantage over methods that rely on such parameters. On the other hand, it constitutes a limitation, as our framework currently cannot directly link the observed absorption enhancement to these fundamental particle properties. For instance, while particle size critically influences the magnitude and spectral dependence of absorption enhancement (e.g., Chen et al., 2025; Fu et al., 2024), our approach does not provide size-resolved insights. To address this, we have provided the aerosol size distribution data, simultaneously measured with a Scanning Mobility Particle Sizer (SMPS), in our accompanying data set (see https://doi.org/10.5281/zenodo.18552344, Shen et al., 2026) for reference by the community. In addition, further work is required to better constrain the influence of BrC chemical composition and filter-based measurement uncertainties, including potential positive and negative artefacts and changes in particle morphology during sampling. Future research efforts are proposed to integrate such size-resolved measurements and multi-component characterizations

(e.g., PAX coupled with a thermal denuder (Cappa et al., 2012; Liu et al., 2015; Pokhrel et al., 2017), SP2 (Dahlkötter et al., 2014), or VTDMA (Zhang et al., 2016)) to better constrain the dependence of absorption enhancement on microphysical and compositional variables.

**Data availability**. The primary data used in this study can be obtained from https://doi.org/10.5281/zenodo.18552344 (Shen et al., 2026). In addition, we include the aerosol size data we simultaneously observed using an SMPS into above data set for reference. Other data utilized in the present study are available from the corresponding author on request.

**Author contributions.** Guorui Zhi and Yuzhe Zhang designed the research. Yi Shen and Guorui Zhi wrote the paper. Yi Shen, Wenjing Jin, Yao Kong, and Yuzhe Zhang carried out the field measurements. Yi Shen, Wenjing Jin, Yao Kong, Yuzhe Zhang, Zhengying Li, and Jianzhong Sun analyzed the data. Yuankai Wang and Zhijian Liang helped with the interpretation of the results.

**Competing interests.** The authors declare that they have no conflict of interest.

**Financial support.** This study was supported by the National Natural Science Foundation of China (grant nos. 42477275, 41977309).

# References


Andre, K., Dlugi, R., and Schnatz, G.: Absorption of Visible Radiation by Atmospheric Aerosol Particles Fog and Cloud Water Residues, J. Atmos. Sci., 38, 141–155, https://doi.org/10.1175/1520-0469(1981)038%3C0141:AOVRBA%3E2.0.CO;2, 1981.

Arhami, M., Shahne, M. Z., Hosseini, V., Roufigar Haghighat, N., Lai, A. M., and Schauer, J. J.: Seasonal trends in the composition and sources of PM2.5 and carbonaceous aerosol in Tehran, Iran, Environ. Pollut., 239, 69–81, https://doi.org/10.1016/j.envpol.2018.03.111, 2018.

Aswini, A. R., Hegde, P., Nair, P. R., and Aryasree, S.: Seasonal changes in carbonaceous aerosols over a tropical coastal location in response to meteorological processes, Sci. Total Environ., 656, 1261–1279, https://doi.org/10.1016/j.scitotenv.2018.11.366, 2019.

Bond, T. C., Doherty, S. J., Fahey, D. W., Forster, P. M., Berntsen, T., DeAngelo, B. J., Flanner, M. G., Ghan, S., Kärcher, B., Koch, D., Kinne, S., Kondo, Y., Quinn, P. K., Sarofim, M. C., Schultz, M. G., Schulz, M., Venkataraman, C., Zhang, H., Zhang, S., Bellouin, N., Guttikunda, S. K., Hopke, P. K., Jacobson, M. Z., Kaiser, J. W., Klimont, Z., Lohmann, U., Schwarz, J. P., Shindell, D., Storelvmo, T., Warren, S. G., and Zender, C. S.: Bounding the role of black carbon in the climate system: A scientific assessment, J. Geophys. Res.-Atmos., 118, 5380–5552, https://doi.org/10.1002/jgrd.50171, 2013.

Bond, T. C., Habib, G., and Bergstrom, R. W.: Limitations in the enhancement of visible light absorption due to mixing state, J. Geophys. Res., 111, D20211, https://doi.org/10.1029/2006JD007315, 2006.

Boonpeng, B., ChooChuay, C., Dejchanchaiwong, R., Tekasakul, P., Nim, N., Bunyarit, C., Choodum, A., Areerob, T., Kleangklao, B., Wandee, S., Pianroj, Y., and Jumrat, S.: An investigation of carbonaceous components and source identification of ultrafine particulate matter in the atmosphere of the southern region of thailand,

583 Aerosol Air Qual. Res., 26, 8, https://doi.org/10.1007/s44408-025-00084-0, 2026.
584 Cappa, C. D., Onasch, T. B., Massoli, P., Worsnop, D. R., Bates, T. S., Cross, E. S.,
585 Davidovits, P., Hakala, J., Hayden, K. L., Jobson, B. T., Kolesar, K. R., Lack, D.
586 A., Lerner, B. M., Li, S.-M., Mellon, D., Nuaaman, I., Olfert, J. S., Petäjä, T.,
587 Quinn, P. K., Song, C., Subramanian, R., Williams, E. J., and Zaveri, R. A.:
588 Radiative absorption enhancements due to the mixing state of atmospheric black
589 carbon, Science, 337, 1078–1081, https://doi.org/10.1126/science.1223447, 2012.
590 Cappa, C. D., Zhang, X., Russell, L. M., Collier, S., Lee, A. K. Y., Chen, C., Betha, R.,
591 Chen, S., Liu, J., Price, D. J., Sanchez, K. J., McMeeking, G. R., Williams, L. R.,
592 Onasch, T. B., Worsnop, D. R., Abbatt, J., and Zhang, Q.: Light absorption by
593 ambient black and brown carbon and its dependence on black carbon coating state
594 for two California, USA, cities in winter and summer, J. Geophys. Res.-Atmos.,
595 124, 1550–1577, https://doi.org/10.1029/2018JD029501, 2019.
596 Chen, B., Bai, Z., Cui, X., Chen, J., Andersson, A., and Gustafsson, Ö.: Light absorption
597 enhancement of black carbon from urban haze in Northern China winter, Environ.
598 Pollut., 221, 418–426, https://doi.org/10.1016/j.envpol.2016.12.004, 2017.
599 Chen, L. W. A., Chow, J. C., Wang, X. L., Robles, J. A., Sumlin, B. J., Lowenthal, D.
600 H., Zimmermann, R., and Watson, J. G.: Multi-wavelength optical measurement
601 to enhance thermal/optical analysis for carbonaceous aerosol, Atmos. Meas. Tech.,
602 8, 451–461, https://doi.org/10.5194/amt-8-451-2015, 2015.
603 Chen, X., Ching, J., Wu, F., Matsui, H., Jacobson, M. Z., Zhang, F., Wang, Y., Zhang,
604 Z., Liu, D., Zhu, S., Rudich, Y., Shi, Z., Yoo, H., Jeon, K.-J., and Li, W.: Locating
605 the missing absorption enhancement due to multi-core black carbon aerosols, Nat.
606 Commun., 16, 10187, https://doi.org/10.1038/s41467-025-65079-2, 2025.
607 Choudhary, V., Rajput, P., Rajeev, P., and Gupta, T.: Synergistic effect in absorption
608 properties of brown carbon and elemental carbon over IGP during weak southwest
609 monsoon, Aerosol Sci. Eng., 1, 138–149, https://doi.org/10.1007/s41810-017-
610 0013-1, 2017.

611 Chow, J. C., Watson, J. G., Chen, L.-W. A., Chang, M. C. O., Robinson, N. F., Trimble,
612 D., and Kohl, S.: The IMPROVE_A Temperature Protocol for Thermal/Optical
613 Carbon Analysis: Maintaining Consistency with a Long-Term Database, Journal
614 of the Air & Waste Management Association, 57, 1014–1023,
615 https://doi.org/10.3155/1047-3289.57.9.1014, 2007.
616 Chow, J. C., Watson, J. G., Green, M. C., Wang, X., Chen, L.-W. A., Trimble, D. L.,
617 Cropper, P. M., Kohl, S. D., and Gronstal, S. B.: Separation of brown carbon from
618 black carbon for IMPROVE and Chemical Speciation Network PM2.5 samples, J.
619 Air Waste Manage., 68, 494–510,
620 https://doi.org/10.1080/10962247.2018.1426653, 2018.
621 Chung, S. H.: Climate response of direct radiative forcing of anthropogenic black
622 carbon, J. Geophys. Res., 110, D11102, https://doi.org/10.1029/2004JD005441,
623 2005.
624 Cui, X., Wang, X., Yang, L., Chen, B., Chen, J., Andersson, A., and Gustafsson, Ö.:
625 Radiative absorption enhancement from coatings on black carbon aerosols, Sci.
626 Total Environ., 551–552, 51–56, https://doi.org/10.1016/j.scitotenv.2016.02.026,
627 2016.
628 Curci, G., Alyuz, U., Barò, R., Bianconi, R., Bieser, J., Christensen, J. H., Colette, A.,
629 Farrow, A., Francis, X., Jiménez-Guerrero, P., Im, U., Liu, P., Manders, A.,
630 Palacios-Peña, L., Prank, M., Pozzoli, L., Sokhi, R., Solazzo, E., Tuccella, P., Unal,
631 A., Vivanco, M. G., Hogrefe, C., and Galmarini, S.: Modelling black carbon
632 absorption of solar radiation: Combining external and internal mixing assumptions,
633 Atmos. Chem. Phys., 19, 181–204, https://doi.org/10.5194/acp-19-181-2019,
634 2019.
635 Dahlkötter, F., Gysel, M., Sauer, D., Minikin, A., Baumann, R., Seifert, P., Ansmann,
636 A., Fromm, M., Voigt, C., and Weinzierl, B.: The Pagami Creek smoke plume after
637 long-range transport to the upper troposphere over Europe – aerosol properties and
638 black carbon mixing state, Atmos. Chem. Phys., 14, 6111–6137,

https://doi.org/10.5194/acp-14-6111-2014, 2014.

Fan, R., Ma, Y., Cao, W., Jin, S., Liu, B., Wang, W., Li, H., and Gong, W.: New insights into black carbon light absorption enhancement: A comprehensive analysis of two differential behaviors, Environ. Pollut., 355, 124175, https://doi.org/10.1016/j.envpol.2024.124175, 2024.

Fierce, L., Bond, T. C., Bauer, S. E., Mena, F., and Riemer, N.: Black carbon absorption at the global scale is affected by particle-scale diversity in composition, Nat. Commun., 7, 12361, https://doi.org/10.1038/ncomms12361, 2016.

Fischer, K.: Bestimmung der Absorption von sichtbarer Strahlung durch Aerosolpartikeln, 1970.

Flanner, M. G., Zender, C. S., Randerson, J. T., and Rasch, P. J.: Present-day climate forcing and response from black carbon in snow, J. Geophys. Res., 112, D11202, https://doi.org/10.1029/2006JD008003, 2007.

Fu, X., Li, X., Zhang, F., Ren, Z., Ge, A., Zhang, X., Fang, Z., Song, W., Deng, W., Zhang, Y., Rudich, Y., and Wang, X.: Evolution of Light Absorption Enhancement of Black Carbon Aerosols From Biomass Burning in Atmospheric Photochemical Aging, J. Geophys. Res.-Atmos., 129, e2024JD040756, https://doi.org/10.1029/2024JD040756, 2024.

Guan, L., Cohen, J. B., Wang, S., Tiwari, P., Liu, Z., and Qin, K.: Improving Aerosol Absorption Estimates Via Size-Resolved Constraints Based on AERONET and In Situ Measurements, Geophysical Research Letters, 53, e2025GL117418, https://doi.org/10.1029/2025GL117418, 2026.

Han, Y. M., Cao, J. J., Lee, S. C., Ho, K. F., and An, Z. S.: Different characteristics of char and soot in the atmosphere and their ratio as an indicator for source identification in Xi'an, China, Atmos. Chem. Phys., 10, 595–607, https://doi.org/10.5194/acp-10-595-2010, 2010.

Han, Y. M., Han, Z. W., Cao, J. J., Chow, J. C., Watson, J. G., An, Z. S., Liu, S. X., and Zhang, R. J.: Distribution and origin of carbonaceous aerosol over a rural high-

667 mountain lake area, Northern China and its transport significance, Atmos. Environ.,
668 42, 2405–2414, https://doi.org/10.1016/j.atmosenv.2007.12.020, 2008.
669 Heintzenberg, J.: Size-segregated measurements of particulate elemental carbon and
670 aerosol light absorption at remote arctic locations, Atmospheric Environment, 16,
671 2461–2469, https://doi.org/10.1016/0004-6981(82)90136-6, 1982.
672 Helin, A., Virkkula, A., Backman, J., Pirjola, L., Sippula, O., Aakko‐Saksa, P.,
673 Väätäinen, S., Mylläri, F., Järvinen, A., Bloss, M., Aurela, M., Jakobi, G.,
674 Karjalainen, P., Zimmermann, R., Jokiniemi, J., Saarikoski, S., Tissari, J., Rönkkö,
675 T., Niemi, J. V., and Timonen, H.: Variation of Absorption Ångström Exponent in
676 Aerosols From Different Emission Sources, JGR Atmospheres, 126,
677 e2020JD034094, https://doi.org/10.1029/2020JD034094, 2021.
678 Hitzenberger, R. and Tohno, S.: Comparison of black carbon (BC) aerosols in two urban
679 areas – concentrations and size distributions, Atmospheric Environment, 35,
680 2153–2167, https://doi.org/10.1016/S1352-2310(00)00480-5, 2001.
681 Hitzenberger, R., Fohler-Norek, C., Dusek, U., Galambos, Z., and Sidla, S.:
682 Comparison of recent (1994) black carbon data with those obtained in 1985 and
683 1986 in the urban area of Vienna, Austria: implications for future environmental
684 policy decisions, Science of The Total Environment, 189–190, 275–280,
685 https://doi.org/10.1016/0048-9697(96)05219-9, 1996.
686 Jacobson, M. Z.: Strong radiative heating due to the mixing state of black carbon in
687 atmospheric aerosols, Nature, 409, 695–697, https://doi.org/10.1038/35055518,
688 2001.
689 Jin, Y., Wang, J., Liu, C., Wong, D. C., Sarwar, G., Fahey, K. M., Wu, S., Wang, J., Cai,
690 J., Tian, Z., Zhang, Z., Xing, J., Ding, A., and Wang, S.: Accounting for the black
691 carbon aging process in a two-way coupled meteorology–air quality model, Atmos.
692 Chem. Phys., 25, 2613–2630, https://doi.org/10.5194/acp-25-2613-2025, 2025.
693 Kaskaoutis, D. G., Grivas, G., Stavroulas, I., Bougiatioti, A., Liakakou, E., Dumka, U.
694 C., Gerasopoulos, E., and Mihalopoulos, N.: Apportionment of black and brown

carbon spectral absorption sources in the urban environment of Athens, Greece, during winter, Sci. Total Environ., 801, 149739, https://doi.org/10.1016/j.scitotenv.2021.149739, 2021.

Kelesidis, G. A., Neubauer, D., Fan, L.-S., Lohmann, U., and Pratsinis, S. E.: Enhanced light absorption and radiative forcing by black carbon agglomerates, Environ. Sci. Technol., 56, 8610–8618, https://doi.org/10.1021/acs.est.2c00428, 2022.

Kong, Y., Zhi, G., Jin, W., Zhang, Y., Shen, Y., Li, Z., Sun, J., and Ren, Y.: A review of quantification methods for light absorption enhancement of black carbon aerosol, Sci. Total Environ., 924, 171539, https://doi.org/10.1016/j.scitotenv.2024.171539, 2024.

Lack, D. A. and Cappa, C. D.: Impact of brown and clear carbon on light absorption enhancement, single scatter albedo and absorption wavelength dependence of black carbon, Atmos. Chem. Phys., 10, 4207–4220, https://doi.org/10.5194/acp-10-4207-2010, 2010.

Lack, D. A. and Langridge, J. M.: On the attribution of black and brown carbon light absorption using the Ångström exponent, Atmos. Chem. Phys., 13, 10535–10543, https://doi.org/10.5194/acp-13-10535-2013, 2013.

Lack, D. A., Langridge, J. M., Bahreini, R., Cappa, C. D., Middlebrook, A. M., and Schwarz, J. P.: Brown carbon and internal mixing in biomass burning particles, P. Natl. Acad. Sci. USA, 109, 14802–14807, https://doi.org/10.1073/pnas.1206575109, 2012.

Laskin, A., Laskin, J., and Nizkorodov, S. A.: Chemistry of atmospheric brown carbon, Chem. Rev., 115, 4335–4382, https://doi.org/10.1021/cr5006167, 2015.

Laskin, A., West, C. P., and Hettiyadura, A. P. S.: Molecular insights into the composition, sources, and aging of atmospheric brown carbon, Chem. Soc. Rev., 54, 1583–1612, https://doi.org/10.1039/D3CS00609C, 2025.

Li, H. Z., Dallmann, T. R., Li, X., Gu, P., and Presto, A. A.: Urban organic aerosol exposure: Spatial variations in composition and source impacts, Environ. Sci.

Technol., 52, 415–426, https://doi.org/10.1021/acs.est.7b03674, 2018.

Li, J., Liu, C., Yin, Y., and Kumar, K. R.: Numerical investigation on the ångström exponent of black carbon aerosol, J. Geophys. Res.-Atmos., 121, 3506–3518, https://doi.org/10.1002/2015JD024718, 2016.

Li, S., Zhang, H., Wang, Z., and Chen, Y.: Advances in the research on brown carbon aerosols: Its concentrations, radiative forcing, and effects on climate, Aerosol Air Qual. Res., 23, 220336, https://doi.org/10.4209/aaqr.220336, 2023a.

Li, Z., Zhi, G., Zhang, Y., Jin, W., Sun, J., Kong, Y., Shen, Y., and Zhang, H.: The integrating sphere system plus in-situ absorption monitoring: A new scheme to study absorption enhancement of black carbon in ambient aerosols, Sci. Total Environ., 892, 164355, https://doi.org/10.1016/j.scitotenv.2023.164355, 2023b.

Liu, B., Zhang, J., Wang, L., Liang, D., Cheng, Y., Wu, J., Bi, X., Feng, Y., Zhang, Y., and Yang, H.: Characteristics and sources of the fine carbonaceous aerosols in Haikou, China, Atmos. Res., 199, 103–112, https://doi.org/10.1016/j.atmosres.2017.08.022, 2018a.

Liu, C., Chung, C. E., Yin, Y., and Schnaiter, M.: The absorption ångström exponent of black carbon: from numerical aspects, Atmos. Chem. Phys., 18, 6259–6273, https://doi.org/10.5194/acp-18-6259-2018, 2018b.

Liu, J., Christensen, J. H., Ye, Z., Dong, S., Geels, C., Brandt, J., Nenes, A., Yuan, Y., and Im, U.: Impact of meteorology and aerosol sources on PM2.5 and oxidative potential variability and levels in China, Atmos. Chem. Phys., 24, 10849–10867, https://doi.org/10.5194/acp-24-10849-2024, 2024.

Liu, S., Aiken, A. C., Gorkowski, K., Dubey, M. K., Cappa, C. D., Williams, L. R., Herndon, S. C., Massoli, P., Fortner, E. C., Chhabra, P. S., Brooks, W. A., Onasch, T. B., Jayne, J. T., Worsnop, D. R., China, S., Sharma, N., Mazzoleni, C., Xu, L., Ng, N. L., Liu, D., Allan, J. D., Lee, J. D., Fleming, Z. L., Mohr, C., Zotter, P., Szidat, S., and Prévôt, A. S. H.: Enhanced light absorption by mixed source black and brown carbon particles in UK winter, Nat. Commun., 6, 8435,

https://doi.org/10.1038/ncomms9435, 2015.

Luo, J., Zhang, Y., and Zhang, Q.: Effects of black carbon morphology on brown carbon absorption estimation: From numerical aspects, Geosci. Model Dev., 14, 2113–2126, https://doi.org/10.5194/gmd-14-2113-2021, 2021.

Luo, J., Zhang, Y., Wang, F., and Zhang, Q.: Effects of brown coatings on the absorption enhancement of black carbon: a numerical investigation, Atmos. Chem. Phys., 18, 16897–16914, https://doi.org/10.5194/acp-18-16897-2018, 2018.

Mbengue, S., Zikova, N., Schwarz, J., Vodička, P., Šmejkalová, A. H., and Holoubek, I.: Mass absorption cross-section and absorption enhancement from long term black and elemental carbon measurements: A rural background station in central Europe, Sci. Total Environ., 794, 148365, https://doi.org/10.1016/j.scitotenv.2021.148365, 2021.

Medalia, A. I., Rivin, D., and Sanders, D. R.: A comparison of carbon black with soot, Science of The Total Environment, 31, 1–22, https://doi.org/10.1016/0048-9697(83)90053-0, 1983.

Moschos, V., Gysel-Beer, M., Modini, R. L., Corbin, J. C., Massabò, D., Costa, C., Danelli, S. G., Vlachou, A., Daellenbach, K. R., Szidat, S., Prati, P., Prévôt, A. S. H., Baltensperger, U., and El Haddad, I.: Source-specific light absorption by carbonaceous components in the complex aerosol matrix from yearly filter-based measurements, Atmos. Chem. Phys., 21, 12809–12833, https://doi.org/10.5194/acp-21-12809-2021, 2021.

Peng, C., Yang, F., Tian, M., Shi, G., Li, L., Huang, R.-J., Yao, X., Luo, B., Zhai, C., and Chen, Y.: Brown carbon aerosol in two megacities in the Sichuan Basin of southwestern China: Light absorption properties and implications, Sci. Total Environ., 719, 137483, https://doi.org/10.1016/j.scitotenv.2020.137483, 2020.

Peng, J., Hu, M., Shang, D., Wu, Z., Du, Z., Tan, T., Wang, Y., Zhang, F., and Zhang, R.: Explosive secondary aerosol formation during severe haze in the North China Plain, Environ. Sci. Technol., 55, 2189–2207,

https://doi.org/10.1021/acs.est.0c07204, 2021.

Penner, J. E., Chuang, C. C., and Grant, K.: Climate forcing by carbonaceous and sulfate aerosols, Clim. Dynam., 14, 839–851, https://doi.org/10.1007/s003820050259, 1998.

Pokhrel, R. P., Beamesderfer, E. R., Wagner, N. L., Langridge, J. M., Lack, D. A., Jayarathne, T., Stone, E. A., Stockwell, C. E., Yokelson, R. J., and Murphy, S. M.: Relative importance of black carbon, brown carbon, and absorption enhancement from clear coatings in biomass burning emissions, Atmos. Chem. Phys., 17, 5063–5078, https://doi.org/10.5194/acp-17-5063-2017, 2017.

Ravindra, K., Singh, T., Mandal, T. K., Sharma, S. K., and Mor, S.: Seasonal variations in carbonaceous species of PM2.5 aerosols at an urban location situated in Indo-Gangetic Plain and its relationship with transport pathways, including the potential sources, J. Environ. Manage., 303, 114049, https://doi.org/10.1016/j.jenvman.2021.114049, 2022.

Reisinger, P., Wonaschütz, A., Hitzenberger, R., Petzold, A., Bauer, H., Jankowski, N., Puxbaum, H., Chi, X., and Maenhaut, W.: Intercomparison of measurement techniques for black or elemental carbon under urban background conditions in wintertime: Influence of biomass combustion, Environ. Sci. Technol., 42, 884–889, https://doi.org/10.1021/es0715041, 2008.

Samset, B. H., Wilcox, L. J., Allen, R. J., Stjern, C. W., Lund, M. T., Ahmadi, S., Ekman, A., Elling, M. T., Fraser-Leach, L., Griffiths, P., Keeble, J., Koshiro, T., Kushner, P., Lewinschal, A., Makkonen, R., Merikanto, J., Nabat, P., Narazenko, L., O'Donnell, D., Oshima, N., Rumbold, S. T., Takemura, T., Tsigaridis, K., and Westervelt, D. M.: East asian aerosol cleanup has likely contributed to the recent acceleration in global warming, Commun Earth Environ, 6, 543, https://doi.org/10.1038/s43247-025-02527-3, 2025.

Schnaiter, M.: Absorption amplification of black carbon internally mixed with secondary organic aerosol, J. Geophys. Res., 110, D19204,

https://doi.org/10.1029/2005JD006046, 2005.

Schwarz, J. P., Spackman, J. R., Fahey, D. W., Gao, R. S., Lohmann, U., Stier, P., Watts, L. A., Thomson, D. S., Lack, D. A., Pfister, L., Mahoney, M. J., Baumgardner, D., Wilson, J. C., and Reeves, J. M.: Coatings and their enhancement of black carbon light absorption in the tropical atmosphere, J. Geophys. Res., 113, D03203, https://doi.org/10.1029/2007JD009042, 2008.

Selimovic, V., Yokelson, R. J., McMeeking, G. R., and Coefield, S.: In situ measurements of trace gases, PM, and aerosol optical properties during the 2017 NW US wildfire smoke event, Atmos. Chem. Phys., 19, 3905–3926, https://doi.org/10.5194/acp-19-3905-2019, 2019.

Shen, Y., Zhi, G., Jin, W., Kong, Y., Zhang, Y., Li, Z., Sun, J., Wang, Y., and Liang, Z.: Beijing air quality and light absorption coefficients dataset 2023 [data set], https://doi.org/10.5281/zenodo.18552344, 2026.

Shiraiwa, M., Kondo, Y., Iwamoto, T., and Kita, K.: Amplification of light absorption of black carbon by organic coating, Aerosol Sci. Tech., 44, 46–54, https://doi.org/10.1080/02786820903357686, 2010.

Song, J., Saathoff, H., Gao, L., Gebhardt, R., Jiang, F., Vallon, M., Bauer, J., Norra, S., and Leisner, T.: Variations of PM2.5 sources in the context of meteorology and seasonality at an urban street canyon in southwest Germany, Atmos. Environ., 282, 119147, https://doi.org/10.1016/j.atmosenv.2022.119147, 2022.

Sun, J., Zhang, Y., Zhi, G., Hitzenberger, R., Jin, W., Chen, Y., Wang, L., Tian, C., Li, Z., Chen, R., Xiao, W., Cheng, Y., Yang, W., Yao, L., Cao, Y., Huang, D., Qiu, Y., Xu, J., Xia, X., Yang, X., Zhang, X., Zong, Z., Song, Y., and Wu, C.: Brown carbon's emission factors and optical characteristics in household biomass burning: developing a novel algorithm for estimating the contribution of brown carbon, Atmos. Chem. Phys., 21, 2329–2341, https://doi.org/10.5194/acp-21-2329-2021, 2021.

Sun, J., Zhi, G., Hitzenberger, R., Chen, Y., Tian, C., Zhang, Y., Feng, Y., Cheng, M.,

Zhang, Y., Cai, J., Chen, F., Qiu, Y., Jiang, Z., Li, J., Zhang, G., and Mo, Y.: Emission factors and light absorption properties of brown carbon from household coal combustion in China, Atmos. Chem. Phys., 17, 4769–4780, https://doi.org/10.5194/acp-17-4769-2017, 2017.

Thuillier, G., Hersé, M., Labs, D., Foujols, T., Peetermans, W., Gillotay, D., Simon, P. C., and Mandel, H.: The Solar Spectral Irradiance from 200 to 2400 nm as Measured by the SOLSPEC Spectrometer from the Atlas and Eureca Missions, Sol. Phys., 214, 1–22, https://doi.org/10.1023/A:1024048429145, 2003.

Tohidi, R., Altuwayjiri, A., and Sioutas, C.: Investigation of organic carbon profiles and sources of coarse PM in los angeles, Environmental Pollution, 314, 120264, https://doi.org/10.1016/j.envpol.2022.120264, 2022.

Wang, L., Jin, W., Sun, J., Zhi, G., Li, Z., Zhang, Y., Guo, S., He, J., and Zhao, C.: Seasonal features of brown carbon in northern China: Implications for BrC emission control, Atmos. Res., 257, 105610, https://doi.org/10.1016/j.atmosres.2021.105610, 2021a.

Wang, Q., Han, Y., Ye, J., Liu, S., Pongpiachan, S., Zhang, N., Han, Y., Tian, J., Wu, C., Long, X., Zhang, Q., Zhang, W., Zhao, Z., and Cao, J.: High contribution of secondary brown carbon to aerosol light absorption in the southeastern margin of Tibetan Plateau, Geophys. Res. Lett., 46, 4962–4970, https://doi.org/10.1029/2019GL082731, 2019a.

Wang, Q., Jacob, D. J., Spackman, J. R., Perring, A. E., Schwarz, J. P., Moteki, N., Marais, E. A., Ge, C., Wang, J., and Barrett, S. R. H.: Global budget and radiative forcing of black carbon aerosol: Constraints from pole-to-pole (HIPPO) observations across the Pacific, J. Geophys. Res.-Atmos., 119, 195–206, https://doi.org/10.1002/2013JD020824, 2014.

Wang, Q., Liu, H., Ye, J., Tian, J., Zhang, T., Zhang, Y., Liu, S., and Cao, J.: Estimating absorption Ångström exponent of black carbon aerosol by coupling multiwavelength absorption with chemical composition, Environ. Sci. Technol.

Lett., 8, 121–127, https://doi.org/10.1021/acs.estlett.0c00829, 2021b.

Wang, Q., Ye, J., Wang, Y., Zhang, T., Ran, W., Wu, Y., Tian, J., Li, L., Zhou, Y., Ho, S. S. H., Dang, B., Zhang, Q., Zhang, R., Chen, Y., Zhu, C., and Cao, J.: Wintertime optical properties of primary and secondary brown carbon at a regional site in the North China Plain, Environ. Sci. Technol., 53, 12389–12397, https://doi.org/10.1021/acs.est.9b03406, 2019b.

Wang, X., Heald, C. L., Liu, J., Weber, R. J., Campuzano-Jost, P., Jimenez, J. L., Schwarz, J. P., and Perring, A. E.: Exploring the observational constraints on the simulation of brown carbon, Atmos. Chem. Phys., 18, 635–653, https://doi.org/10.5194/acp-18-635-2018, 2018.

Wonaschütz, A., Hitzenberger, R., Bauer, H., Pouresmaeil, P., Klatzer, B., Caseiro, A., and Puxbaum, H.: Application of the integrating sphere method to separate the contributions of brown and black carbon in atmospheric aerosols, Environ. Sci. Technol., 43, 1141–1146, https://doi.org/10.1021/es8008503, 2009.

Wu, G., Ram, K., Fu, P., Wang, W., Zhang, Y., Liu, X., Stone, E. A., Pradhan, B. B., Dangol, P. M., Panday, A. K., Wan, X., Bai, Z., Kang, S., Zhang, Q., and Cong, Z.: Water-soluble brown carbon in atmospheric aerosols from Godavari (Nepal), a regional representative of South Asia, Environ. Sci. Technol., 53, 3471–3479, https://doi.org/10.1021/acs.est.9b00596, 2019.

Wu, G.-M., Cong, Z.-Y., Kang, S.-C., Kawamura, K., Fu, P.-Q., Zhang, Y.-L., Wan, X., Gao, S.-P., and Liu, B.: Brown carbon in the cryosphere: Current knowledge and perspective, Adv. Clim. Change Res., 7, 82–89, https://doi.org/10.1016/j.accre.2016.06.002, 2016a.

Wu, Y., Zhang, R., Tian, P., Tao, J., Hsu, S.-C., Yan, P., Wang, Q., Cao, J., Zhang, X., and Xia, X.: Effect of ambient humidity on the light absorption amplification of black carbon in Beijing during January 2013, Atmos. Environ., 124, 217–223, https://doi.org/10.1016/j.atmosenv.2015.04.041, 2016b.

Xie, C., Xu, W., Wang, J., Liu, D., Ge, X., Zhang, Q., Wang, Q., Du, W., Zhao, J., Zhou,

W., Li, J., Fu, P., Wang, Z., Worsnop, D., and Sun, Y.: Light absorption enhancement of black carbon in urban Beijing in summer, Atmos. Environ., 213, 499–504, https://doi.org/10.1016/j.atmosenv.2019.06.041, 2019.

Xie, Y., Zeng, L., Hu, S., Wang, T., Du, Z., Tan, T., Xu, N., Chen, S., Mao, J., Xu, F., and Hu, M.: Long-term trends of black carbon levels, sources, and radiative effects from 2013 to 2022 in Beijing, China, npj Clim. Atmos. Sci., 1, 10, https://doi.org/10.1038/s44407-025-00010-z, 2025.

Xu, X., Zhao, W., Zhang, Q., Wang, S., Fang, B., Chen, W., Venables, D. S., Wang, X., Pu, W., Wang, X., Gao, X., and Zhang, W.: Optical properties of atmospheric fine particles near Beijing during the HOPE-J$^3$A campaign, Atmos. Chem. Phys., 16, 6421–6439, https://doi.org/10.5194/acp-16-6421-2016, 2016.

Yang, S., Liu, Y., Chen, L., Cao, N., Wang, J., and Gao, S.: Direct radiative forcing of light-absorbing carbonaceous aerosol and the influencing factors over China, Atmos. Chem. Phys., 25, 9335–9355, https://doi.org/10.5194/acp-25-9335-2025, 2025.

Yue, S., Bikkina, S., Gao, M., Barrie, L. A., Kawamura, K., and Fu, P.: Sources and radiative absorption of water-soluble brown carbon in the high Arctic atmosphere, Geophys. Res. Lett., 46, 14881–14891, https://doi.org/10.1029/2019GL085318, 2019.

Yus-Díez, J., Via, M., Alastuey, A., Karanasiou, A., Minguillón, M. C., Perez, N., Querol, X., Reche, C., Ivančič, M., Rigler, M., and Pandolfi, M.: Absorption enhancement of black carbon particles in a Mediterranean city and countryside: Effect of particulate matter chemistry, ageing and trend analysis, Atmos. Chem. Phys., 22, 8439–8456, https://doi.org/10.5194/acp-22-8439-2022, 2022.

Zhang, R., Khalizov, A. F., Pagels, J., Zhang, D., Xue, H., and McMurry, P. H.: Variability in morphology, hygroscopicity, and optical properties of soot aerosols during atmospheric processing, P. Natl. Acad. Sci. USA, 105, 10291–10296, https://doi.org/10.1073/pnas.0804860105, 2008.

Zhang, X., Mao, M., Chen, H., Yin, Y., and Tang, S.: Lensing effect of black carbon with brown coatings: Dominant microphysics and parameterization, J. Geophys. Res.-Atmos., 126, e2020JD033549, https://doi.org/10.1029/2020JD033549, 2021.

Zhang, X., Mao, M., Yin, Y., and Tang, S.: The absorption Ångstrom exponent of black carbon with brown coatings: effects of aerosol microphysics and parameterization, Atmos. Chem. Phys., 20, 9701–9711, https://doi.org/10.5194/acp-20-9701-2020, 2020.

Zhang, Y., Zhang, Q., Cheng, Y., Su, H., Kecorius, S., Wang, Z., Wu, Z., Hu, M., Zhu, T., Wiedensohler, A., and He, K.: Measuring the morphology and density of internally mixed black carbon with SP2 and VTDMA: new insight into the absorption enhancement of black carbon in the atmosphere, Atmos. Meas. Tech., 9, 1833–1843, https://doi.org/10.5194/amt-9-1833-2016, 2016.

Zhang, Y., Zhi, G., Jin, W., Wang, L., Guo, S., Shi, R., Sun, J., Cheng, M., Bi, F., Gao, J., Zhang, B., Wu, J., Shi, Z., Liu, B., Wang, Z., and Li, S.: Differing effects of escalating pollution on absorption and scattering efficiencies of aerosols: Toward co-beneficial air quality enhancement and climate protection measures, Atmos. Environ., 232, 117570, https://doi.org/10.1016/j.atmosenv.2020.117570, 2020.

Zhang, Y., Zhi, G., Tian, C., Li, S., Sun, J., Zhang, Y., and Yang, T.: Study of the details of aerosol carbon measurements in autumn and winter in Beijing, Environ. Sci. Res., 30, 1184–1192, https://doi.org/10.13198/j.issn.1001-6929.2017.02.56, 2017.

Zhao, G., Tan, T., Zhu, Y., Hu, M., and Zhao, C.: Method to quantify black carbon aerosol light absorption enhancement with a mixing state index, Atmos. Chem. Phys., 21, 18055–18063, https://doi.org/10.5194/acp-21-18055-2021, 2021.

Zhi, G., Chen, Y., Xue, Z., Meng, F., Cai, J., Sheng, G., and Fu, J.: Comparison of elemental and black carbon measurements during normal and heavy haze periods: implications for research, Environ. Monit. Assess., 186, 6097–6106, https://doi.org/10.1007/s10661-014-3842-2, 2014.

Zhu, C., Qu, Y., Huang, H., Chen, J., Dai, W., Huang, R., and Cao, J.: Black carbon and

947 secondary brown carbon, the dominant light absorption and direct radiative forcing
948 contributors of the atmospheric aerosols over the Tibetan Plateau, Geophys. Res.
949 Lett., 48, e2021GL092524, https://doi.org/10.1029/2021GL092524, 2021.
950